

See discussions, stats, and author profiles for this publication at: <https://www.researchgate.net/publication/265419534>

Mechanisms of Failure in Nanoscale Metallic Glass

ARTICLE *in* NANO LETTERS · SEPTEMBER 2014

Impact Factor: 13.59 · DOI: 10.1021/nl5027869 · Source: PubMed

CITATIONS

9

READS

160

7 AUTHORS, INCLUDING:



[Mehdi Jafary-Zadeh](#)

Institute Of High Performance Computing

11 PUBLICATIONS 36 CITATIONS

[SEE PROFILE](#)



[David Z. Chen](#)

California Institute of Technology

14 PUBLICATIONS 1,538 CITATIONS

[SEE PROFILE](#)



[Julia R. Greer](#)

California Institute of Technology

108 PUBLICATIONS 3,753 CITATIONS

[SEE PROFILE](#)

Mechanisms of Failure in Nanoscale Metallic Glass

X. Wendy Gu,[†] Mehdi Jafary-Zadeh,[§] David Z. Chen,[‡] Zhaoxuan Wu,[§] Yong-Wei Zhang,[§] David J. Srolovitz,^{||} and Julia R. Greer*,[‡]

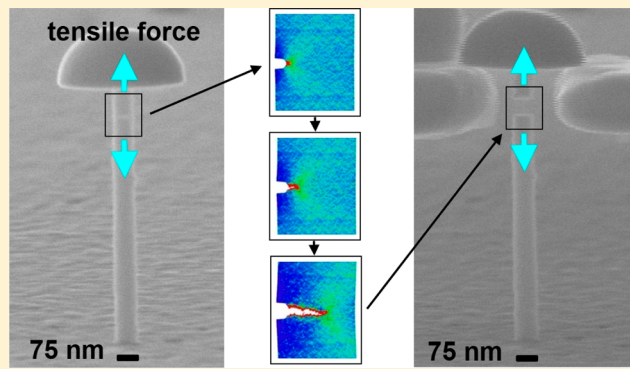
[†]Division of Chemistry and Chemical Engineering and [‡]Division of Engineering and Applied Science, California Institute of Technology, 1200 E. California Blvd., Pasadena, California 91125, United States

[§]Institute of High Performance Computing, 1 Fusionopolis Way, #16-16 Connexis, Singapore 138632

^{||}Departments of Materials Science and Engineering & Mechanical Engineering and Applied Mechanics, University of Pennsylvania, Philadelphia, Pennsylvania 19104, United States

Supporting Information

ABSTRACT: The emergence of size-dependent mechanical strength in nanosized materials is now well-established, but no fundamental understanding of fracture toughness or flaw sensitivity in nanostructures exists. We report the fabrication and *in situ* fracture testing of ~70 nm diameter Ni–P metallic glass samples with a structural flaw. Failure occurs at the structural flaw in all cases, and the failure strength of flawed samples was reduced by 40% compared to unflawed samples. We explore deformation and failure mechanisms in a similar nanometallic glass via molecular dynamics simulations, which corroborate sensitivity to flaws and reveal that the structural flaw shifts the failure mechanism from shear banding to cavitation. We find that failure strength and deformation in amorphous nanosolids depend critically on the presence of flaws.



KEYWORDS: Size effect, metallic glass, notch sensitivity, flaw sensitivity, mechanical properties, fracture, molecular dynamics

Nanomaterials have been lauded for performance enhancements in applications as diverse as energy,^{1,2} electronics,^{3,4} biotechnology⁵ and even structural materials.^{6,7} Understanding nanoscale mechanics is critical for the implementation of nanomaterials in all applications (even where the application is not primarily structural) since a minimum level of mechanical robustness is necessary for prolonged operation. Many engineering materials show enhanced strength,^{8,9} ductility (in intrinsically brittle materials),^{10,11} and fracture toughness¹² when shrunk to the nanoscale. This leads to the possibility of designing strong and tough functional materials based on nanostructural building blocks. Such design principles are widely applied in nature where hard biomaterials like crustacean shells, radiolaria, and spider silk simultaneously possess remarkable strength and toughness.¹³

One class of promising nanosized structural materials is metallic glass because of its high strength and enhanced ductility compared to the bulk.^{11,14,15} The fracture behavior and toughness of nanometallic glasses must also be evaluated; unpredictable catastrophic failure has been an outstanding issue that has prevented the widespread insertion of bulk metallic glasses into devices and composites.^{16–18} Recent work suggests that the tensile strength of bulk and nanoscale metallic glasses may be insensitive to notches.^{19,20} The observed notch insensitivity at the nanoscale may be related to the concept

of nanoscale flaw tolerance, a continuum-based theory which suggests that the strength of intrinsically brittle materials approaches its theoretical limit and does not diminish due to the presence of flaws when the sample size is reduced to a critical length scale on the order of hundreds of nanometers.²¹ The theory of flaw tolerance at the nanoscale can also be applied to materials which exhibit limited plastic deformation for small yielding conditions.²² These observations provide the impetus for an in-depth investigation of local stresses at the notch root and the mechanisms of failure in nanoscale metallic glasses.

Our earlier work on fracture in ~100 nm nanocrystalline Pt nanotensile samples with prefabricated flaws revealed flaw-insensitivity in strength and flaw-sensitivity of failure localization.²³ Experiments and MD simulations showed that these behaviors stem from the competition between stress concentrations at the structural flaw (external) and at discrete microstructural features such as grain boundaries (internal). Although structural flaws serve as strong stress concentrators and generally govern failure location, plasticity within the grains in nanocrystalline metals reduce the stress at the flaw to the level of the stress concentrators of microstructural origin within

Received: July 22, 2014

Revised: September 3, 2014

the structure. The fracture strengths of all nc-Pt samples were similar regardless of whether failure occurred at the structural flaw or within the microstructure. This fracture behavior arises from the combination of the discrete stress landscape within the nanocrystalline microstructure and the nanoscale sample size.²³

Flaw-insensitivity in strength was observed when microstructural stress concentrations (e.g., grain boundaries and triple junctions) superseded the stress concentrations associated with structural flaws.^{23–25} By this argument, strength should be sensitive to structural flaws in the absence of microstructural stress concentrations, such as in the case of the nanosized metallic glass samples studied in this work. The intrinsic mechanical length scale in metallic glasses is associated with clusters of ~100 atoms (i.e., a few atomic diameters in size) that serve as shear transformation zones (STZs) upon deformation. Beyond this nearly atomic scale, metallic glasses exhibit a homogeneous internal energy landscape. This means that an external stress concentrator, such as a structural flaw, should determine failure location, strength, and mechanism when the length scale of the stress concentrator exceeds the size of this atomic-level, internal stress fluctuation. In this work, we focus on elucidating the mechanisms of failure in nanoscale metallic glass containing a structural flaw through experimental nanomechanical testing and molecular dynamics simulations.

Ni–P metallic glass nanostructures were electroplated into a poly(methyl methacrylate) (PMMA) thin film that was patterned with an array of 70–75 nm-diameter holes using e-beam lithography (Figure 1A).²⁶ A gold layer underneath the

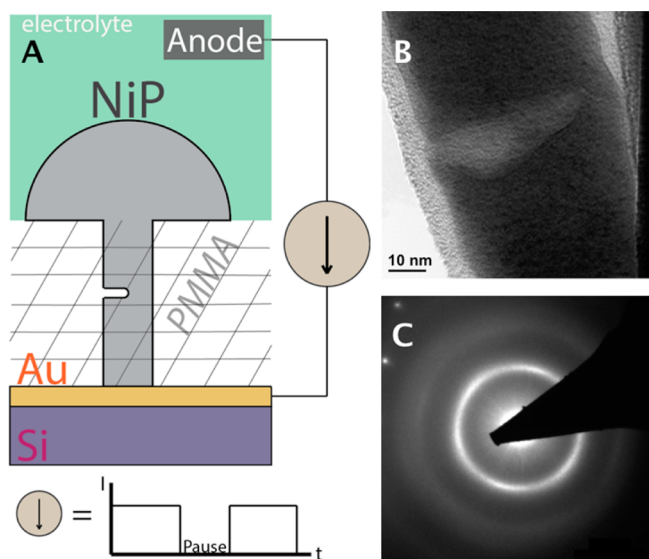


Figure 1. (A) Schematic of templated electroplating of notched Ni–P nanocylinders using a “paused” electroplating method. (B) Bright field TEM image of the notched region in a Ni–P nanocylinder. (C) Corresponding electron diffraction pattern showing the amorphous nature of the nanocylinder. Single crystal diffraction peaks are due to the Cu TEM grid supporting the nanocylinder.

PMMA layer served as the cathode for electroplating. A 75 at. % Ni–25 at. % P metallic glass was plated by applying a 80 mA/cm² current between the Au-PMMA electrode and a Ni counter electrode in a nickel sulfate-based aqueous bath as described in Chen et al.¹⁴ Cylindrical nanocylinders were formed by plating continuously for 35 s. Notched metallic glass nanocylinders were formed by first plating into a template

continuously for 15 s, followed by four successive 5 s periods interrupted by ~10 min pauses.²³ The plating was continued until the metallic glass nanocylinders began to overgrow the PMMA thin film surface. The PMMA layer was removed after the electroplating process to leave freestanding cylindrical tensile testing samples with protrusions at the ends that serve as tension grips.

The sample and notch geometries were characterized using scanning electron microscopy (SEM) (FEI Quanta). The notched cylindrical samples had diameters of 69 ± 2 nm and lengths of 851 ± 11 nm. The notches appear as thin lines when imaged in SEM at 20 kV, so the resolution of these observations were limited to features above ~10 nm. Despite this limited resolution, small variations in notch length and height were observed qualitatively. The imaging conditions resulted in an electron beam penetration depth that was a significant fraction of the cylinder diameter and images of the notch include information both from the surface and from within the cylinder. All notched samples were fabricated using a paused electroplating methodology and contained a notch 768 ± 10 nm from the base of the cylinder. Three of the seven nanocylinders that were tested contained an additional notch at 638 ± 12 nm from the base of the cylinder. Unnotched nanocylinders with diameters of 74 ± 3 nm and lengths of 434 ± 10 nm were also fabricated. The difference in the dimensions of the notched and unnotched samples was caused by variations in the e-beam lithographed templates used to create these samples.

Transmission electron microscopy (TEM) was used to obtain higher resolution images of the notches and to analyze the microstructure of the nanocylinder. Samples were transferred from the growth substrate to a Cu TEM half-grid with minimal mechanical perturbation and no focused ion beam (FIB) damage (details of TEM sample preparation are included in the Supporting Information). Bright- and dark-field TEM images and electron diffraction patterns confirmed that the nanoscale metallic glass samples were amorphous (Figure 1B and C).¹⁴ A small amount of ordering was observed and is likely associated with crystallinity within the e-beam deposited C and W layers on the surface of the Ni–P nanocylinder. The spots visible in the upper left corner of the diffraction pattern in Figure 1C are associated with the Cu TEM grid supporting the nanocylinders. The notch shown in Figure 1B has a height of 10 nm and a rounded notch root similar to that shown schematically in Figure 1A. The width and depth of the notch could not be accurately measured using the TEM because of difficulties distinguishing between surface features and those within the nanostructure. Qualitatively, the TEM images revealed that the notch extends a significant distance across the diameter of the sample and that the structure is thinner at the notch than at surrounding areas based on diffraction contrast. No change in the amorphous structure between the notch region and the rest of the structure was observed.

In situ SEM uniaxial tension tests were performed at a nominal strain rate of 0.001 s⁻¹ on notched and unnotched Ni–P nanocylinders using the InSEM system.²⁷ Unnotched Ni–P samples were glued to the substrate using a small amount of e-beam deposited W (Nova 200, FEI) (Figure 2A). It was not necessary to glue notched Ni–P samples because they always broke within the cylindrical gauge length at stresses lower than the interfacial strength between the sample and the underlying substrate (Figure 2C). Videos of the in situ SEM

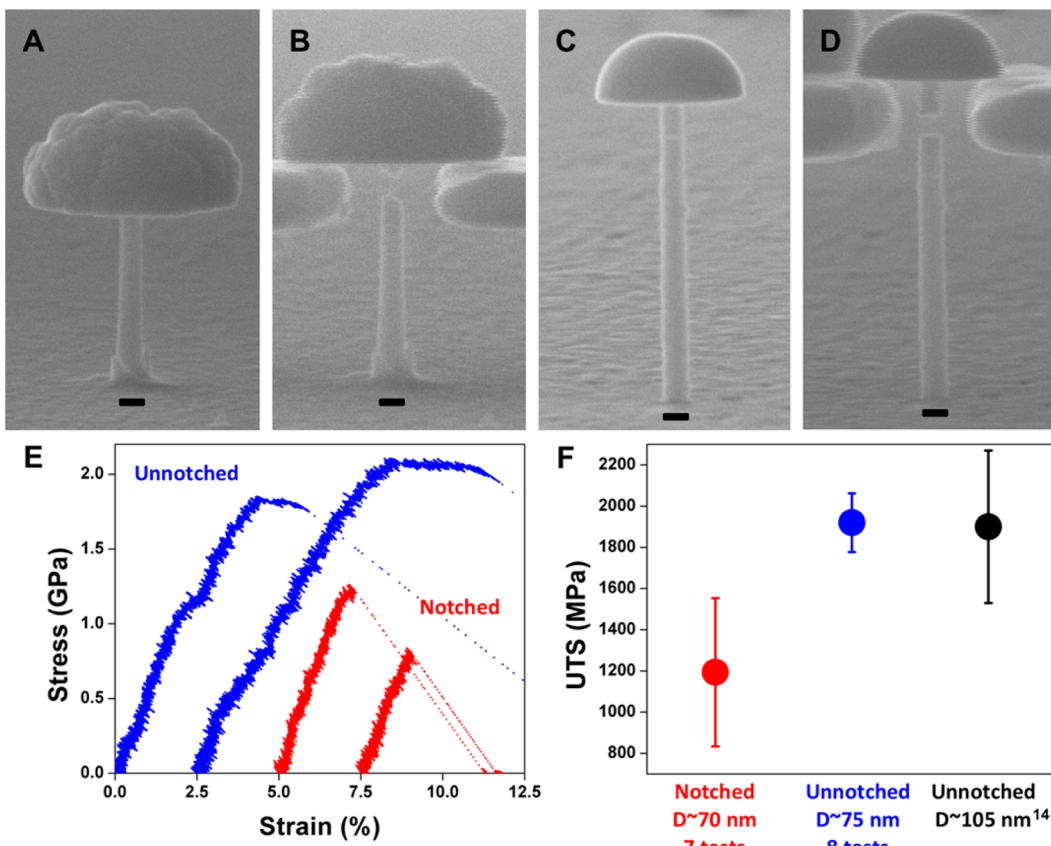


Figure 2. SEM images of an unnotched Ni–P nanocylinder (A) before and (B) after tensile testing and a notched Ni–P nanocylinder (C) before and (D) after tensile testing. The scale bar represents 75 nm. (E) Characteristic stress–strain curves for notched (red) and unnotched Ni–P nanocylinders (blue). (F) Comparison of the UTS of notched and unnotched Ni–P nanocylinders with ~ 70 nm diameters and unnotched Ni–P nanocylinders with a ~ 105 nm diameter.¹⁴

mechanical experiments can be found in the Supporting Information.

Unnotched, ~ 75 nm diameter Ni–P nanocylinders showed $\sim 3\%$ post-elastic deformation in tension in contrast with the brittle failure observed in wider Ni–P metallic glass samples of the same composition.¹⁴ The ultimate tensile strength (UTS) of the eight tested unnotched cylinders was 1.9 ± 0.1 GPa, consistent with previously reported strengths of thicker, 105 nm diameter Ni–P metallic glass nanocylinders.¹⁴ Failure in the unnotched samples occurred through necking, followed by shear banding resulting in an angled fracture surface (Figure 2B). The fracture planes were inclined, on average, by $\sim 25^\circ$ relative to the loading axis but showed variation in the 5 – 42° range, as measured from the SEM images. We note that, because the fracture surface was not always aligned with the viewing direction, the values reported here should be considered lower bounds on the fracture angle for each sample.

The notched Ni–P nanocylinders always broke at the notch. Their average failure stress, 1.2 ± 0.4 GPa, was significantly lower than that of the unnotched nanocylinders. Six of the seven tested notched samples broke at an UTS lower than that of the unnotched pillars. One notched pillar broke at an UTS of 1.9 GPa. Notched samples that failed at ~ 1.2 GPa exhibited limited plastic strain, 0.3%, as compared to 3% plastic strain in the unnotched nanocylinders (Figure 2E). This is a clear demonstration that the stress concentration at the notch plays a key role in the deformation mode. Nanoscale metallic glasses have previously been shown to exhibit increased ductility, but

no increases in strength when reduced below ~ 100 nm in size.^{11,28} If the only role of the notch was to decrease the effective diameter and the cross-sectional area of the nanocylinder, then increasing the notch size should lead to higher ductility. Figure 2F proves that the Ni–P samples are in a size-independent regime with regards to strength, because decreasing the unnotched sample diameter from ~ 105 nm to ~ 75 nm does not change the UTS (~ 1.9 GPa in both cases). The decrease in UTS observed in the notched ~ 70 nm samples (~ 1.2 GPa) must be due to the effect of the notch rather than due to a reduction in the sample diameter.

The fracture surface in the notched samples was inclined 4° relative to the loading axis on average, with all samples breaking at angles within the 0 – 10° range (Figure 2D). Part of the observed “fracture surface” may, in fact, be the surface of the notch; this is difficult to quantify because the notch sizes could not be precisely determined.

To elucidate the physical origin of the effect of the notch on failure, we performed large-scale molecular dynamics (MD) simulations on notched and unnotched Fe₇₅P₂₅ metallic glass nanocylinders. The atomic interactions within the Fe–P metallic glass were modeled using the embedded atom method (EAM) potential parametrized by Ackland et al.²⁹ We focus on Fe–P metallic glasses rather than Ni–P glasses here because no Ni–P potentials that have been validated against measured mechanical properties of Ni–P are available, while one does exist for Fe–P. Iron and nickel have similar electronegativity: both are transition metals from the same row of the periodic

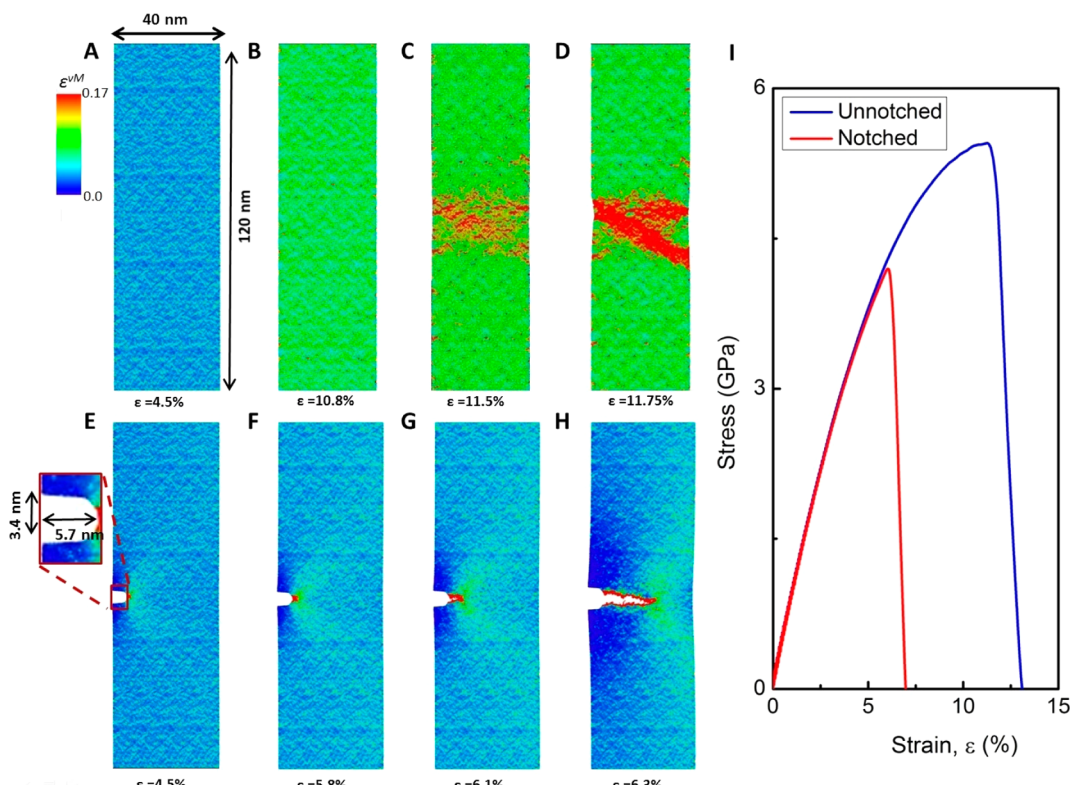


Figure 3. MD simulation results with the atoms shaded according to their von Mises strain ϵ^{vM} in a cross-section of the unnotched sample at (A) $\epsilon = 4.5\%$ (uniform ϵ^{vM}), (B) $\epsilon = 10.8\%$ (strain at ultimate tensile stress), (C) $\epsilon = 11.5\%$ (at the inception of shear band), and (D) $\epsilon = 11.75\%$ (well-developed shear band). For comparison, ϵ^{vM} is plotted for the notched sample at (E) $\epsilon = 4.5\%$ (elevated local strain at the notch), (F) $\epsilon = 5.8\%$ (strain at the ultimate tensile stress and beginning of crack formation), (G) $\epsilon = 6.1\%$ (crack propagates horizontally), and (H) $\epsilon = 6.3\%$ (failure via crack propagation). (I) Stress–strain curves corresponding to the simulated tensile tests of unnotched and notched amorphous samples.

table, and the bonding in Fe₇₅P₂₅ and Ni₇₅P₂₅ is very similar. On this basis, we expect that Fe–P is a reasonable surrogate for Ni–P for MD simulations. However, like for MD simulations based upon any type of empirical potentials, the details of the predictions should be viewed with some skepticism. The high strain rate used in the MD simulations ($5 \times 10^7 \text{ s}^{-1}$) may also influence observed deformation mechanisms. For these reasons, we focus on major mechanistic features and trends in behavior when interpreting MD simulation results.

Simulations were performed using the large-scale atomic/molecular massively parallel simulator (LAMMPS).³⁰ Details of the molecular dynamics simulations are provided in the Supporting Information. The simulated unnotched samples were constructed as cylinders with a diameter of 40 nm and a length of 120 nm (Figure 3A). The notched sample was formed by cutting a rounded notch with length of 5.7 nm and height of 3.4 nm out of the unnotched sample (Figure 3E). Deformation and failure of the simulation samples were analyzed in terms of the local atomic von Mises shear strain, ϵ^{vM} .^{31,32} Visualization of ϵ^{vM} has been widely used to investigate shear band (SB) formation in metallic glasses.³¹ Figure 3A–H show ϵ^{vM} for a central cross section of representative unnotched and notched nanocylinders at different applied strains, ϵ . Figure 3A–D show that the distribution of ϵ^{vM} in the unnotched sample is uniform up to the UTS, which corresponds to $\epsilon_{\text{unnotched}}^{\text{UTS}} \sim 10.8\%$. Beyond the UTS, a shear band forms, which leads to failure at an oblique angle ($\sim 45^\circ$) relative to the loading direction. The notched nanocylinder does not fail through shear banding, but instead fails by crack initiation and propagation from the notch root after reaching the UTS (Figure 3E–H). The crack

propagates from the notch in a direction orthogonal to the applied load. The engineering stress–strain data for both the unnotched and notched nanocylinders are shown in Figure 3I. The UTS for the unnotched and notched samples is attained at applied strains of $\epsilon_{\text{unnotched}}^{\text{UTS}} \sim 10.8\%$ and $\epsilon_{\text{notched}}^{\text{UTS}} \sim 5.8\%$, respectively. The UTS of the notched sample was $\sim 25\%$ lower than that of the unnotched sample. MD tensile test videos can be found in the Supporting Information.

The MD simulations appear to be in excellent agreement with the experimental observations and unambiguously demonstrate that the notch governs the failure mode and mechanism in nanoscale metallic glasses. Both simulations and experiments show that the unnotched nanocylinders failed in a ductile fashion via shear banding, with the fracture surface oriented at an oblique angle with respect to the loading axis. The notched nanocylinders failed in a brittle manner via crack propagation from near the notch root, horizontally across the sample. The tensile strength of the notched sample was significantly smaller than that of the unnotched sample in both experiments (36% reduction) and simulations (25% reduction). The observed reduction in strength and transition in failure mode indicate that the notched metallic glass nanocylinders are notch sensitive.

MD simulations were previously performed on Cu–Zr nanoscale metallic glasses in which failure always initiated from rounded flaws.²⁰ Our results agree with these simulations in fracture location but not in failure strength. The load at fracture was normalized by the cross-sectional area at the flaw to obtain a normalized UTS in the Cu–Zr metallic glass nanoscale sample. This normalized failure strength was found to be

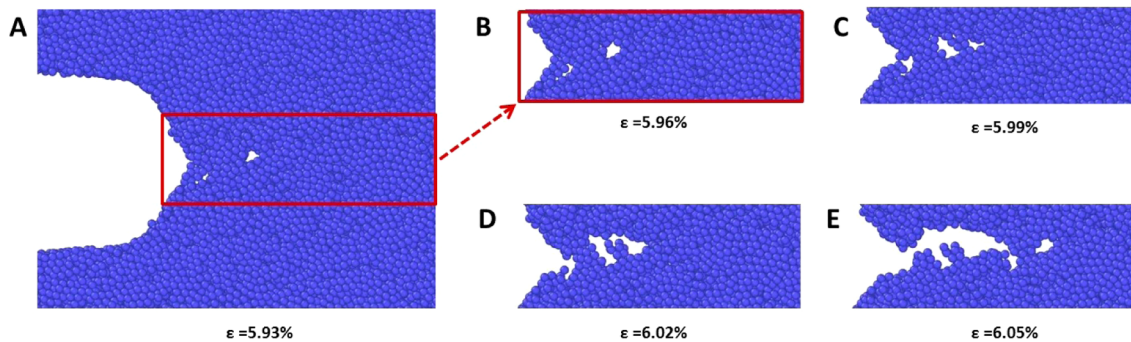


Figure 4. Detailed view of the deformation in the notched sample showing (A) formation of atom-scale voids ($\varepsilon = 5.93\%$), (B) growth of voids ($\varepsilon = 5.96\%$), continued growth of voids and formation of additional voids at (C) $\varepsilon = 5.99\%$ and (D) $\varepsilon = 6.02\%$, and (E) coalescence of voids ($\varepsilon = 6.05\%$). Images show a cross-section of the simulation nanocylinder.

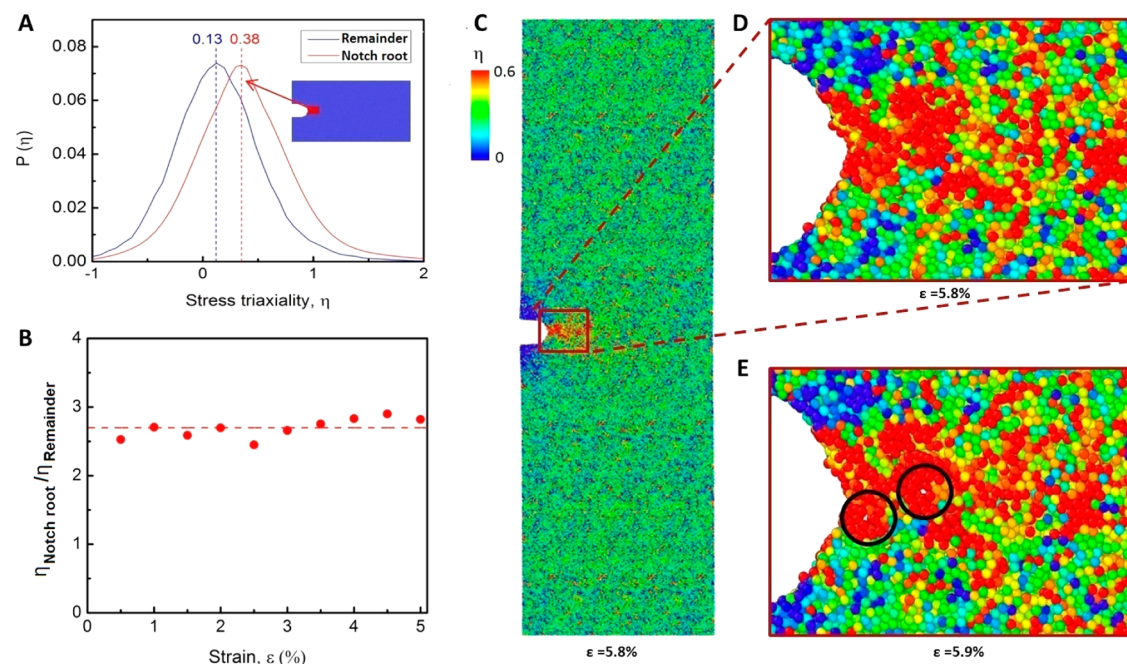


Figure 5. (A) Plot of the probability density of the stress triaxiality, $P(\eta)$, at the notch root (red curve) in comparison with the $P(\eta)$ for the remainder of the sample (blue curve) at an applied strain of $\varepsilon = 4.5\%$. $P(\eta)$ is calculated for a 2 nm thick slice through the cylindrical sample. The $P(\eta)$ at the notch root is calculated for the region located in front of the notch root (red area in the inset). The data for the remainder of the sample are calculated for all other atoms in the sample (blue region in inset). (B) The normalized value of average stress triaxiality, $\eta_{\text{notch-root}}/\eta_{\text{remainder}}$, as a function of applied strain, ε . The spatial distribution of η in (C) the cross section of the notched nanocylinder at the strain corresponding to the UTS, (D) near the notch at the UTS, and (E) near the notch at a slightly higher strain $\varepsilon = 5.9\%$. Voids nucleate at the notch root due to high localized η (indicated by the black circles).

independent of notch size. The notch in the Fe–P metallic glass nanocylinders reduces the cross-sectional area of the cylindrical sample by 9%, but reduces its strength by 25%, which indicates notch-sensitivity at the nanoscale in this material. This difference in behavior is indicative of a difference in the underlying mechanism of failure between notched Cu–Zr and notched Fe–P glasses.³³ Cu–Zr deforms through shear banding that initiates at the notch,²⁰ while notched Fe–P fails through void formation and growth as shown in Figure 4. The plastic shear banding in Cu–Zr is able to relieve stress at the notch such that the stress concentration at the notch has a negligible effect on failure strength. Similarly, stable shear bands propagate from notches in certain bulk metallic glasses which serves to strengthen the metallic glass and lead to notch insensitivity.¹⁹ The stress relaxation mechanism of shear

banding is unavailable to notched Fe–P so flaw sensitivity is observed instead.

Figure 4A–E shows several close-up views of the notch root region at different stages of loading. Microscopic voids were nucleated in front of the notch root at an applied strain of $\varepsilon = 5.93\%$, a value slightly above $\varepsilon_{\text{notched}}^{\text{UTS}} \sim 5.8\%$, and subsequently grew while additional small voids emerged (Figure 4A–C). The coalescence of these voids and their linkup with the dominant crack led to crack propagation (see Figure 4D–E) and eventually caused fracture and the formation of a horizontal fracture surface (see movie in the Supporting Information). Although fracture is microscopically ductile (because it occurs through void nucleation, growth and coalescence), the overall failure process can be viewed as brittle crack propagation because the total amount of plastic deformation is very small.

We postulate that the observed cavitation was caused by the substantial stress triaxiality ahead of the notch. The atomic stress triaxiality is defined as $\eta = Tr(\sigma)/3\sigma^{vM}$, where σ is the atomic stress tensor. When η is large, hydrostatic stress dominates, leading to void nucleation and growth. When η is small, shear deformation dominates, and shear banding is expected.^{34,35} We calculated η in both the notch root region (red region in the inset of Figure 5A), as well as for the whole sample excluding the notch root area (blue region in Figure 5A). Figure 5A shows $P(\eta)$, the stress triaxiality distribution in the notch root area (red curve) in comparison with that for the remainder of the sample (blue curve) at an applied strain of $\epsilon = 4.5\%$. It is seen that η at the notch root is shifted toward more positive values and its average increased by almost 300% to 0.38 (red dash line) from $\eta = 0.13$ as compared with the rest of the sample (blue dashed line). Figure 5B shows the normalized value of average stress triaxiality, $\eta_{\text{notch-root}}/\eta_{\text{remainder}}$, as a function of applied strain, ϵ . This figure indicates that during the uniaxial tensile test, there is a much greater degree of volumetric expansion at the notch root as compared with rest of the sample, which drives the nucleation and growth of the voids. Figure 5C–D shows the spatial distribution of η in the cross-section of the notched nanocylinder at the UTS (corresponding to $\epsilon = 5.8\%$). Much higher values of η are observed in front of the notch root. Voids are nucleated in these regions of large η near the notch root at a very small increment in the applied strain (to 5.9%), as seen in Figure 5E.

Our results indicate that flaws are critical to the failure strength and failure mechanism in this nanoscale metallic glass. Recent theory suggests the emergence of flaw tolerance in solids at very small length scales which applies directly to brittle materials.²¹ The amorphous system examined here shows nontrivial localized plasticity through either shear banding or voiding. The present observations demonstrate that the effects of flaws are consistent with classical analyses and that these are remarkably robust—applicable down to the scale of the smallest man-made mechanical structures. While our earlier work showed that nanocrystalline metals can be flaw-tolerant in terms of strength,²³ this work conveys that the flaw tolerance is associated with the specific discrete microstructure rather than with the nanoscale sample size. The absence of a discrete microstructure, as is the case for the amorphous metallic glasses in this work, implies no flaw-tolerance in nanoscale materials that exhibit localized plasticity.

In summary, we explored the deformation mechanism and failure modes of notched and unnotched amorphous metallic glass nanostructures under uniaxial tension in experiment and atomistic simulation. Structural flaws reduce sample failure strength and are critical to the failure location and failure mode. In the unnotched nanocylinders, shear band formation led to failure at an oblique angle with respect to the loading direction. The notched nanocylinders showed virtually no ductility and failed via crack initiation and propagation along the extension of the notch root. We found that the nominally brittle propagation of cracks in the notched samples was a consequence of void nucleation, growth, and coalescence in response to the large stress triaxiality at the notch root. This work unambiguously demonstrates that the deformation mode and failure strength of nanostructures depends sensitively on the presence of structural flaws, even in the absence of discrete microstructural features. These findings demonstrate that flaw-insensitivity is not a general feature of nanoscale mechanical systems; classical models that describe the effects of flaws on

failure can be applied at the nanoscale provided that localized plasticity can readily occur. An important caveat is that, even when localized plasticity is possible, discrete microstructural features in nanocrystalline materials can lead to internal stress concentrations that make material strength flaw-insensitive. Future nanotechnologists must take flaw-sensitivity at the nanoscale into account when designing the mechanical aspects of nanostructured materials and devices.

■ ASSOCIATED CONTENT

§ Supporting Information

Descriptions of TEM sample preparation and MD simulation samples, and experimental and MD simulation movies of samples deformed in tension. This material is available free of charge via the Internet at <http://pubs.acs.org>.

■ AUTHOR INFORMATION

Corresponding Author

*Address: M/C 309-81, Division of Engineering and Applied Science, California Institute of Technology, 1200 E. California Blvd., Pasadena, CA 91125, United States. Phone: 626-395-4127. E-mail: jgreer@caltech.edu.

Notes

The authors declare no competing financial interest.

■ ACKNOWLEDGMENTS

X.W.G. thanks the National Defense Science and Engineering Graduate Fellowship, and D.Z.C. thanks the National Science Foundation Graduate Research Fellowship for financial support. J.R.G. acknowledges the National Science Foundation (DMR-1204864). The authors are very grateful to the Kavli Nanoscience Institute at Caltech for the availability of critical cleanroom facilities, Carol Garland for TEM assistance, Rachel Lontas for electroplating templates, and Boyu Fan and Timothy Tsang for help with electroplating. M.J.Z., Z.X.W., and Y.W.Z. gratefully acknowledge the financial support from the Agency for Science, Technology and Research (A*STAR), Singapore and the use of computing resources at the A*STAR Computational Resource Centre, Singapore.

■ REFERENCES

- (1) Polman, A.; Atwater, H. A. *Nat. Mater.* **2012**, *11*, 174–177.
- (2) Boukai, A. I.; Bunimovich, Y.; Tahir-Kheli, J.; Yu, J. K.; Goddard, W. A.; Heath, J. R. *Nature* **2008**, *451*, 168–171.
- (3) Huang, Y.; Duan, X. F.; Cui, Y.; Lauhon, L. J.; Kim, K. H.; Lieber, C. M. *Science* **2001**, *294*, 1313–1317.
- (4) Cui, Y.; Lieber, C. M. *Science* **2001**, *291*, 851–853.
- (5) Bruchez, M.; Moronne, M.; Gin, P.; Weiss, S.; Alivisatos, A. P. *Science* **1998**, *281*, 2013–2016.
- (6) Hao, S. J.; Cui, L. S.; Jiang, D. Q.; Han, X. D.; Ren, Y.; Jiang, J.; Liu, Y. N.; Liu, Z. Y.; Mao, S. C.; Wang, Y. D.; Li, Y.; Ren, X. B.; Ding, X. D.; Wang, S.; Yu, C.; Shi, X. B.; Du, M. S.; Yang, F.; Zheng, Y. J.; Zhang, Z.; Li, X. D.; Brown, D. E.; Li, J. *Science* **2013**, *339*, 1191–1194.
- (7) Schaedler, T. A.; Jacobsen, A. J.; Torrents, A.; Sorensen, A. E.; Lian, J.; Greer, J. R.; Valdevit, L.; Carter, W. B. *Science* **2011**, *334*, 962–965.
- (8) Uchic, M. D.; Dimiduk, D. M.; Florando, J. N.; Nix, W. D. *Science* **2004**, *305*, 986–989.
- (9) Greer, J. R.; De Hosson, J. T. M. *Prog. Mater. Sci.* **2011**, *56*, 654–724.
- (10) Chan, C. K.; Peng, H. L.; Liu, G.; McIlwrath, K.; Zhang, X. F.; Huggins, R. A.; Cui, Y. *Nat. Nanotechnol.* **2008**, *3*, 31–35.
- (11) Jang, D. C.; Greer, J. R. *Nat. Mater.* **2010**, *9*, 215–219.

- (12) Beaber, A. R.; Nowak, J. D.; Ugurlu, O.; Mook, W. M.; Girshick, S. L.; Ballarini, R.; Gerberich, W. W. *Philos. Mag.* **2011**, *91*, 1179–1189.
- (13) Meyers, M. A.; McKittrick, J.; Chen, P. Y. *Science* **2013**, *339*, 773–779.
- (14) Chen, D. Z.; Jang, D.; Guan, K. M.; An, Q.; Goddard, W. A., 3rd; Greer, J. R. *Nano Lett.* **2013**, *13*, 4462–4468.
- (15) Magagnosc, D. J.; Ehrbar, R.; Kumar, G.; He, M. R.; Schroers, J.; Gianola, D. S. *Sci. Rep.* **2013**, *3*, 1–6.
- (16) Hofmann, D. C.; Suh, J. Y.; Wiest, A.; Duan, G.; Lind, M. L.; Demetriou, M. D.; Johnson, W. L. *Nature* **2008**, *451*, 1085–U1083.
- (17) Ritchie, R. O. *Nat. Mater.* **2011**, *10*, 817–822.
- (18) Schuh, C. A.; Hufnagel, T. C.; Ramamurty, U. *Acta Mater.* **2007**, *55*, 4067–4109.
- (19) Qu, R. T.; Calin, M.; Eckert, J.; Zhang, Z. F. *Scr. Mater.* **2012**, *66*, 733–736.
- (20) Sha, Z. D.; Pei, Q. X.; Sorkin, V.; Branicio, P. S.; Zhang, Y. W.; Gao, H. *J. Appl. Phys. Lett.* **2013**, *103*, 081903.
- (21) Gao, H. J.; Ji, B. H.; Jager, I. L.; Arzt, E.; Fratzl, P. *Proc. Natl. Acad. Sci. U.S.A.* **2003**, *100*, 5597–5600.
- (22) Gao, H. J.; Chen, S. H. *J. Appl. Mech.-Trans. ASME* **2005**, *72*, 732–737.
- (23) Gu, X. W.; Wu, Z. X.; Zhang, Y. W.; Srolovitz, D. J.; Greer, J. R. *Nano Lett.* **2013**, *13*, 5703–5709.
- (24) Kumar, S.; Haque, M. A.; Gao, H. *Appl. Phys. Lett.* **2009**, *94*, 253104.
- (25) Zhang, T.; Li, X. Y.; Kadkhodaei, S.; Gao, H. *J. Nano Lett.* **2012**, *12*, 4605–4610.
- (26) Burek, M. J.; Greer, J. R. *Nano Lett.* **2010**, *10*, 69–76.
- (27) Kim, J. Y.; Jang, D. C.; Greer, J. R. *Scr. Mater.* **2009**, *61*, 300–303.
- (28) Volkert, C. A.; Donohue, A.; Spaepen, F. *J. Appl. Phys.* **2008**, *103*, 083539.
- (29) Ackland, G.; Mendelev, M.; Srolovitz, D.; Han, S.; Barashev, A. *J. Phys.: Condens. Matter* **2004**, *16*, S2629.
- (30) Plimpton, S. *J. Comput. Phys.* **1995**, *117*, 1–19.
- (31) Shimizu, F.; Ogata, S.; Li, J. *Mater. T.* **2007**, *48*, 2923–2927.
- (32) Stukowski, A. *Modell. Simul. Mater. Sci. Eng.* **2010**, *18*, 015012.
- (33) Murali, P.; Guo, T. F.; Zhang, Y. W.; Narasimhan, R.; Li, Y.; Gao, H. *J. Phys. Rev. Lett.* **2011**, *107*, 215501.
- (34) Needleman, A. *J. Appl. Mech.-Trans. ASME* **1987**, *54*, 525–531.
- (35) Seppala, E. T.; Belak, J.; Rudd, R. E. *Phys. Rev. B* **2004**, *69*, 134101.